

NUMERICAL SIMULATION OF COEXTRUSION AND FILM CASTING

A. FORTIN and P. CARRIER

Département de Mathématiques Appliquées, École Polytechnique de Montréal, CP 6079, Succursale Centre-Ville, Montréal, H3C 3A7, Canada

AND

Y. DEMAY

Institut Non-linéaire de Nice, 1361 Route des Lucioles, Sophia-Antipolis, F-06560 Valbonne, France

SUMMARY

In the first part of this paper a numerical strategy is developed for the numerical simulation of the coextrusion process. Coextrusion consists of extruding many polymers in the same die in order to combine their respective properties. The die is generally flat and quite large and consequently a two-dimensional approximation is sufficient. The main difficulty is to accurately predict the interfaces between the different layers of polymers. A finite element method based on a pseudoconcentration function is developed to calculate these fluid interfaces. Numerical results are presented for the coextrusion of up to five fluids.

In the second part of the paper the above strategy is slightly modified to simulate the film-casting process. In this case a polymer is stretched (with a draw velocity U_d) at the exit of the die in order to produce a very thin layer of polymer that is cooled in contact with a chill roll. Only one polymer-air interface has to be computed. The draw ratio is defined as $Dr = U_d/\bar{U}$, where \bar{U} is the mean velocity of the polymer at the exit of the die. As the draw ratio is increased, instabilities appear and numerical results put in evidence the draw resonance phenomenon.

KEY WORDS Coextrusion Film casting Finite element Pseudoconcentration

1. INTRODUCTION

Polymers are omnipresent. They are used in the aerospace industry, in automobiles and in a large number of everyday objects. Many processes exist in the polymer industry. One of them is the coextrusion process, which is particularly important in the wrapping industry. The idea is to combine many non-miscible polymers to obtain a product with specific properties such as impermeability, aesthetic quality, resistance, etc. In that specific case the molten polymers are extruded in a flat die. The main difficulty of this process is to balance the flow in order to obtain optimal thicknesses for each layer of polymer. These thicknesses will strongly depend on the shear-thinning behaviour of the polymers and on the different flow rates imposed at the inlet of the die.¹

To compute fluid interfaces, at least two strategies are possible: tracking and capturing. The first strategy tracks the interface and requires full or partial remeshing of the domain in order to follow the interfaces. Consequently, the mesh evolves until it matches the different interfaces. The reader is referred to Reference 2 for an application of the tracking method to the numerical

prediction of extrudate swell. This method requires very efficient remeshing techniques and does not seem to be well adapted for time-dependent problems.

On the other hand, the capturing strategy requires a single mesh and the different interfaces are determined by a function S (often called the pseudoconcentration) which is computed in the whole domain. This, however, requires the solution of a supplementary partial differential equation of hyperbolic type of the form

$$\frac{\partial}{\partial t} S(\vec{x}, t) + (\vec{u} \cdot \vec{\nabla}) S(\vec{x}, t) = 0 \quad \forall \vec{x} \in \Omega,$$

where $\vec{u} = (u_1(\vec{x}), u_2(\vec{x}))$ is the velocity field. This strategy was adopted in the volume-of-fluid (VOF) method of Hirt and Nichols³ and in the pseudoconcentration method of Thompson.⁴ The reader is referred to the excellent paper of Shen⁵ for a review of these methods in the context of injection moulding.

In this paper a capturing strategy is adopted, since we are interested in both stationary and time-dependent problems.^{1,6,7} The discontinuous Galerkin method is used for the computation of the pseudoconcentration function. Numerical results show the accuracy and flexibility of the proposed method.

Let us now present the equations governing the movement of the polymer and the interface positions.

2. EQUATIONS

2.1. Stokes problem

In these simulations inertia and gravitational forces are neglected, as is the case for most polymer-processing applications.⁸ Moreover, surface tension is not taken into account at fluid interfaces since it is generally negligible in the two applications under study. Consequently, the momentum equations can be written as

$$\vec{\nabla} \cdot \boldsymbol{\sigma} = 0, \tag{1}$$

where $\boldsymbol{\sigma}$ is the Cauchy stress tensor defined by

$$\boldsymbol{\sigma} = -p\mathbf{I} + \boldsymbol{\tau}. \tag{2}$$

The extra-stress tensor $\boldsymbol{\tau}$ is related to the velocity field by the relation⁹

$$\boldsymbol{\tau} = 2\eta(|\dot{\boldsymbol{\gamma}}|)\dot{\boldsymbol{\gamma}}(\vec{u}), \tag{3}$$

where $\dot{\boldsymbol{\gamma}}(\vec{u}) = \frac{1}{2}[\vec{\nabla}\vec{u} + (\vec{\nabla}\vec{u})^T]$ is the rate-of-deformation tensor and $|\dot{\boldsymbol{\gamma}}| = \dot{\gamma}_{ij}\dot{\gamma}_{ji}$ is its norm (the Einstein notation has been used). One can remark that the viscosity η depends on the norm of the rate-of-deformation tensor, $|\dot{\boldsymbol{\gamma}}|$, expressing the shear-thinning behaviour of polymers.

Different models exist, all based on experimental data, to take into account shear-thinning effects. Figure 1 illustrates three of these models: the Newtonian law, the power law and the Carreau model. The last one is the most general because it follows experimental data on a wider range of rate of deformation. The viscosity law has the form

$$\eta(|\dot{\boldsymbol{\gamma}}|) = \eta_0(c + \lambda^2|\dot{\boldsymbol{\gamma}}|^2)^{(n-1)/2}, \tag{4}$$

where the Carreau law corresponds to $c = 1$. Usually λ , η_0 and n are determined from experimental data through curve fitting. The power law is obtained by setting $c = 0$, while the Newtonian law corresponds to $n = 1$ (constant viscosity).

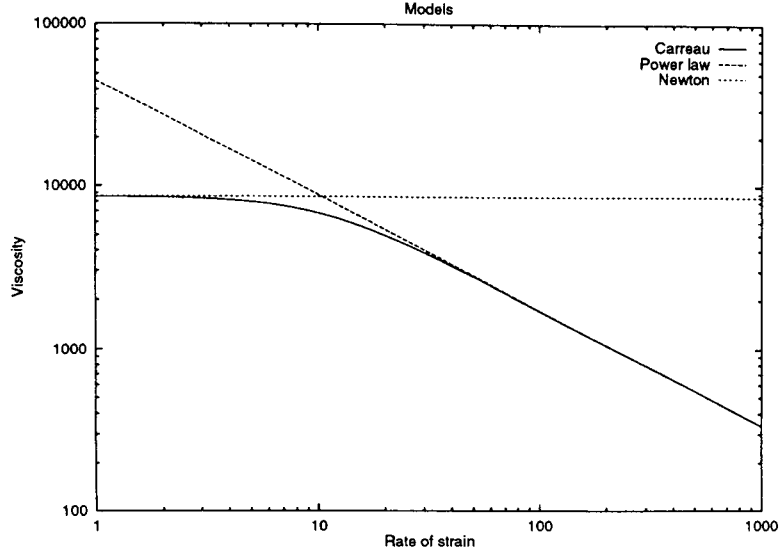


Figure 1. Viscosity models

Combining all these properties, the problem to solve becomes

$$2\vec{\nabla} \cdot (\eta(|\dot{\gamma}|)\dot{\gamma}(\vec{u})) = \vec{\nabla} p, \quad (5)$$

together with the incompressibility condition

$$\vec{\nabla} \cdot \vec{u} = 0. \quad (6)$$

Finally, a supplementary equation is needed to determine the position of the interface between any two molten polymers. This position is determined by a transport equation described in the next subsection.

2.2. The pseudoconcentration method

For the sake of completeness let us recall the basic assumptions of the pseudoconcentration method introduced by Thompson^{4,10} and which presents similarities with the volume-of-fluid method of Hirt and Nichols.³

At polymer interfaces two conditions are to be satisfied. The first one merely states that the interface is at equilibrium and can be written as

$$\sigma_1 \cdot \vec{n} = \sigma_2 \cdot \vec{n}, \quad (7)$$

where σ_i , $i = 1, 2$, is the Cauchy stress tensor on each side of the interface and \vec{n} is the normal vector. This condition will be a direct consequence of the variational formulation, as will be discussed in Section 3.

The second condition on the interface expresses the non-miscibility of the polymers. Suppose that two polymers are coextruded. The general case is similar. They are separated by the interface \mathcal{H} which is *a priori* unknown. Figure 2 illustrates the domain. One can define a function $S(\vec{x}, t)$ in the whole domain Ω by setting

$$S(\vec{x}, t) = \begin{cases} 1 & \text{if } \vec{x} \in \Omega_1, \\ 0 & \text{if } \vec{x} \in \Omega_2. \end{cases} \quad (8)$$

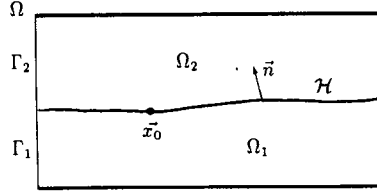


Figure 2. Domain with two fluids

This function is called the pseudoconcentration. The position of the interface is at the jump of the function S (see Figure 2).

To compute the pseudoconcentration, let us consider an initial volume \mathcal{V}^0 in Ω containing the same particles at any time. At time t the volume \mathcal{V}^0 is allowed to deform with the flow and to become \mathcal{V}^t . Any particle inside \mathcal{V}^0 at $t = 0$ will remain in \mathcal{V}^t at time t . Consequently,

$$\frac{d}{dt} \int_{\mathcal{V}^t} S(\vec{x}, t) dx dy = 0. \quad (9)$$

One can show¹¹ that

$$\frac{d}{dt} \int_{\mathcal{V}^t} S(\vec{x}, t) dx dy = \int_{\mathcal{V}^t} \frac{D}{Dt} S(\vec{x}, t) dx dy, \quad (10)$$

where $D/Dt = \partial/\partial t + (\vec{u} \cdot \vec{\nabla})$. Since this is true for all \mathcal{V}^0 (and thus for all \mathcal{V}^t), we get the condition

$$\frac{\partial}{\partial t} S(\vec{x}, t) + (\vec{u} \cdot \vec{\nabla}) S(\vec{x}, t) = 0 \quad \forall \vec{x} \in \Omega. \quad (11)$$

This relation is valid in the entire domain Ω . In other words, the solution of this transport equation (12) is equivalent to the non-miscibility condition and also determines the position of the interface between the two fluids. This is done by searching the jump in the function S . From a practical standpoint, one looks for the isovalue $\frac{1}{2}$ of the function S .

For the coextrusion problem, only stationary solutions are of interest and the time derivative term is neglected. The equation reduces to

$$(\vec{u} \cdot \vec{\nabla}) S(\vec{x}) = 0 \quad \forall \vec{x} \in \Omega. \quad (12)$$

However, for film-casting problems,^{12,13} time-dependent solutions arise after the onset of the instabilities and in that case the time derivative will be discretized by a fully implicit Gear scheme which can be written as

$$\frac{\partial S(\vec{x}, t_{n+1})}{\partial t} \simeq \frac{3S(\vec{x}, t_{n+1}) - 4S(\vec{x}, t_n) + S(\vec{x}, t_{n-1})}{2\Delta t}. \quad (13)$$

The Gear scheme is second-order in time and has been proven to be very accurate for the prediction of time-dependent problems.¹⁴

2.3. Boundary conditions

Suppose p fluids are coextruded in a very simple flat die like the one in Figure 3. Then $\Omega = \cup_{k=1}^p \Omega_k$. The interfaces are between each domain Ω_k , $k = 1, \dots, p-1$, and their positions are *a priori* unknown.

Boundary conditions for the velocity field must be provided on each of the Γ_k . This is a delicate question, since the flow can be rather complex before entering the die. However, since viscoelastic effects are neglected, the developed velocity profile in the die should not depend on the precise form of the imposed velocity profile on Γ_k . The interfaces depend strongly, however, on the respective flow rates Q^k in each layer of polymer. Consequently, parabolic profiles with given flow rates Q^k are imposed on each Γ_k . Flat profiles with the same flow rates would give similar results.

A no-slip condition is imposed on each plate Γ_b at the top and bottom of the die. At the die exit the flow, and thus the interface, is supposed fully developed.

To summarize, the boundary conditions are

$$\begin{aligned} \vec{u}^k &= Q^k(u_0^k(y), 0), \quad \vec{x} \in \Gamma_k, \quad k = 1, \dots, p, \\ \vec{u} &= 0, \quad \vec{x} \in \Gamma_b, \\ u_2 &= 0 \quad \text{and} \quad (\boldsymbol{\sigma} \cdot \vec{n})_x = 0, \quad \vec{x} \in \Gamma_s, \end{aligned} \quad (14)$$

where $u_0^k(y)$ are parabolic profiles with unit flow rate. In this manner the flow rates in each layer can be easily changed and their effects on the interfaces can be put in evidence.

For the transport equation (12) a boundary condition must be provided only on the inflow part of the boundary defined as

$$\partial\Omega^- = \{\vec{x} \in \Omega \mid \vec{u}(\vec{x}) \cdot \vec{n}(\vec{x}) < 0\}. \quad (15)$$

The inflow boundary value of S will be transported in all the domain by the velocity field \vec{u} . The different fluids are distinguished by setting S to different values on $\Gamma_1, \dots, \Gamma_p$ (thus the name pseudoconcentration). The following choice was used:

$$S^k = \frac{p-k}{p-1}, \quad \vec{x} \in \Gamma_k, \quad k = 1, \dots, p, \quad (16)$$

with $p \geq 2$. The different jumps in the step function (16) will give the position of the interfaces.

Finally, the equilibrium of the interface,

$$\boldsymbol{\sigma}^k \cdot \vec{n} = \boldsymbol{\sigma}^{k+1} \cdot \vec{n}, \quad \vec{x} \in \mathcal{H}^k, \quad k = 1, \dots, p-1, \quad (17)$$

is automatically satisfied by the variational formulation, as we shall see in Section 3.

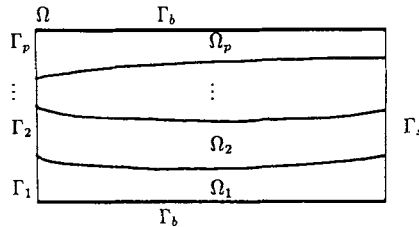


Figure 3. Boundary conditions for coextrusion

3. VARIATIONAL FORMULATIONS

Appropriate variational formulations are needed for both the generalized Stokes problem and the transport equation for the pseudoconcentration:

$$2\bar{\nabla} \cdot (\eta(|\dot{\gamma}|)\dot{\gamma}(\bar{u})) = \bar{\nabla} p, \quad \bar{\nabla} \cdot \bar{u} = 0, \quad (u \cdot \bar{\nabla})S = 0. \quad (18)$$

System (18) is a coupled problem for the three unknowns (\bar{u}, p, S) . To avoid the assembly and factorization of a huge matrix and to take advantage of the discontinuous Galerkin method which allows the solution of the transport equation on an element-by-element basis, a Picard-type iterative scheme will be used to solve this system. Variational formulations are then needed for both the generalized Stokes problem and the transport equation.

3.1. The generalized Stokes problem

Let us suppose at this time that S is known (from a previous iteration, for example). From the value of S it is possible to determine the domain Ω_k where the k th fluid is located.

The boundary of Ω is separated into two parts corresponding to essential (Γ_{ess}) and natural (Γ_{nat}) boundary conditions. Thus $\Gamma = \Gamma_{\text{ess}} \cup \Gamma_{\text{nat}}$ and we take $\bar{v} \in H_{\Gamma_{\text{ess}}}^1(\Omega)^2$ defined by

$$\begin{aligned} H_{\Gamma_{\text{ess}}}^1(\Omega)^2 &= \{\bar{v} \in H^1(\Omega)^2 \mid \bar{v} = \hat{0} \text{ on } \Gamma_{\text{ess}}\}, \\ H^1(\Omega)^2 &= \left\{ \bar{v} \in \mathcal{L}^2(\Omega)^2 \mid \int_{\Omega} \bar{\nabla} \bar{v} : \bar{\nabla} \bar{v} < \infty \right\}, \\ \mathcal{L}^2(\Omega) &= \left\{ q \mid \int_{\Omega} q \cdot q < \infty \right\}. \end{aligned}$$

The momentum equation is then multiplied by $\bar{v} \in H_{\Gamma_{\text{ess}}}^1(\Omega)^2$ and integrated by parts, while the incompressibility condition is multiplied by $q \in \mathcal{L}^2(\Omega)$ and integrated over the domain. This yields the following variational formulation for the generalized Stokes problem:

$$\begin{aligned} \sum_{k=1}^p \left(\int_{\Omega_k} 2\eta_k(|\dot{\gamma}|)(\dot{\gamma}(\bar{u})) : \dot{\gamma}(\bar{v}) \, d\Omega - \int_{\Gamma_{\text{nat}}} (\sigma_k \cdot \bar{n}) \cdot \bar{v} \, d\Gamma - \int_{\Omega_k} (\bar{\nabla} \cdot \bar{v}) p_k \, d\Omega \right) &= 0 \quad \forall \bar{v} \in H_{\Gamma_{\text{ess}}}^1(\Omega)^2, \quad (19) \\ \int_{\Omega} (\bar{\nabla} \cdot \bar{u}) q \, d\Omega &= 0 \quad \forall q \in \mathcal{L}^2(\Omega), \end{aligned}$$

with the viscosity model for the k th fluid given by

$$\eta_k(|\dot{\gamma}|) = \eta_0^k (c_k + \lambda_k^2 |\dot{\gamma}|^2)^{(n_k - 1)/2}. \quad (20)$$

3.1.1. Equilibrium of the interfaces. As already mentioned, the equilibrium condition $\sigma^k \cdot \bar{n} = \sigma^{k+1} \cdot \bar{n}$ is natural with this formulation. Indeed, let us consider the domain of Figure 2. Taking successively $\bar{v} \in \mathcal{D}(\Omega_1)$ and $\bar{v} \in \mathcal{D}(\Omega_2)$, where $\Omega = \Omega_1 \cup \Omega_2$ and where $\mathcal{D}(\Omega_i)$, $i = 1, 2$, is the space of infinitely differentiable functions with compact support, and integrating by parts on Ω_1 and Ω_2 separately, we get the formulations

$$-\int_{\Omega_i} \bar{\nabla} \cdot (2\eta_i(|\dot{\gamma}|)\dot{\gamma}(\bar{u})) \cdot \bar{v} \, d\Omega + \int_{\Omega_i} \bar{\nabla} p_i \cdot \bar{v} \, d\Omega = 0, \quad i = 1, 2, \quad (21)$$

which means that the momentum equations are satisfied in the distribution sense in each domain Ω_i , $i = 1, 2$. Taking now $\bar{v} \in H_{\Gamma_{\text{ess}}}^1(\Omega)^2$ and integrating by parts with \bar{n} fixed arbitrarily as

pointing outwards from Ω_1 , i.e. $\tilde{n} = \tilde{n}_1 = -\tilde{m}_2$, we get

$$\begin{aligned} \sum_{i=1}^2 \left(- \int_{\Omega_i} \tilde{\nabla} \cdot (2\eta_i(|\dot{\gamma}|)\dot{\gamma}(\tilde{u})) \cdot \tilde{v} \, d\Omega + \int_{\Omega_i} (\tilde{\nabla} p_i \cdot \tilde{v}) \, d\Omega \right) + \int_{\mathcal{H}} [2(\eta_1(|\dot{\gamma}|) - \eta_2(|\dot{\gamma}|))\dot{\gamma}(\tilde{u}) \cdot \tilde{n}] \cdot \tilde{v} \, dS \\ - \int_{\mathcal{H}} [(p_1 - p_2)\mathbf{I} \cdot \tilde{n}] \cdot \tilde{v} \, dS = 0. \end{aligned} \quad (22)$$

The first two terms in the summation vanish, since the momentum equation is satisfied in each domain. Using the definition of $\boldsymbol{\sigma}$ (see (2)), we get

$$\int_{\mathcal{H}} [(\boldsymbol{\sigma}^1 - \boldsymbol{\sigma}^2) \cdot \tilde{n}] \cdot \tilde{v} \, d\Omega = 0 \quad \forall \tilde{v} \in H_{\Gamma_{\text{ess}}}^1(\Omega)^2, \quad (23)$$

which is equivalent to

$$\boldsymbol{\sigma}_1 \cdot \tilde{n} = \boldsymbol{\sigma}_2 \cdot \tilde{n} \quad \forall \tilde{x} \in \mathcal{H}. \quad (24)$$

3.1.2. Linearization of the Stokes problem. The variational formulation (19) is non-linear owing to the viscosity model. Moreover, it is constrained by the incompressibility condition. A combination of the Newton–Raphson method and the Uzawa algorithm was used to solve Stokes-type problems as described in References 15 and 16. The Newton–Raphson method takes care of the non-linearities and the Uzawa algorithm enforces the incompressibility condition. This gives the following algorithm:

$$\begin{aligned} \int_{\Omega} 2\eta_0(c + \lambda^2|\dot{\gamma}(\tilde{u}_i)|^2)^{(n-1)/2}(\dot{\gamma}(\delta\tilde{u}_i) : \dot{\gamma}(\tilde{v})) \, d\Omega + 2(n-1)\eta_0 \int_{\Omega} (c + \lambda^2|\dot{\gamma}(\tilde{u}_i)|^2)^{(n-3)/2} \\ \times (\dot{\gamma}(\tilde{u}_i) : \dot{\gamma}(\delta\tilde{u}_i))(\dot{\gamma}(\tilde{u}_i) : \dot{\gamma}(\tilde{v})) \, d\Omega + r \int_{\Omega} (\tilde{\nabla} \cdot \delta\tilde{u}_i)(\tilde{\nabla} \cdot \tilde{v}) \, d\Omega = F(\tilde{u}_i, p_i) + r \int_{\Omega} (\tilde{\nabla} \cdot \tilde{u}_i)\tilde{\nabla} \cdot \tilde{v} \, d\Omega, \\ \tilde{u}_{i+1} = \tilde{u}_i - \delta\tilde{u}_i, p_{i+1} = p_i - r\tilde{\nabla} \cdot \tilde{u}_{i+1}, \quad \text{if } |\delta\tilde{u}_i| < \varepsilon \quad \text{and} \quad |\tilde{\nabla} \cdot \tilde{u}_{i+1}| < \varepsilon, \text{ stop}, \end{aligned} \quad (25)$$

where F is the residual defined by

$$F(\tilde{u}_i, p_i) = 2 \int_{\Omega} \eta(|\dot{\gamma}(\tilde{u}_i)|)\dot{\gamma}(\tilde{u}_i) : \dot{\gamma}(\tilde{v}) \, d\Omega - \int_{\Gamma_{\text{nat}}} (\boldsymbol{\sigma} \cdot \tilde{n}) \cdot \tilde{v} \, dS - \int_{\Omega} (\tilde{\nabla} \cdot \tilde{v})p_i \, d\Omega, \quad (26)$$

r is a penalization parameter and ‘:’ stands for the double contraction product of two tensors.

In the variational formulation (25) we have not indicated the different domains Ω_k for simplicity. In fact, the rheological parameters c , λ and n are functions of the pseudoconcentration S . Since S is known, when computing the elementary matrices, the value of S is evaluated at each Gauss point and its value identifies the polymer. The viscosity coefficient then takes the value of the corresponding polymer.

3.2. The transport equation

A variational formulation is also required for the transport equation (12). We now thus suppose that \tilde{u} is given.

The solution of the transport equation needs to be very accurate since it determines the position of the interfaces. Transport equations are particularly difficult to solve when discontinuous solutions are present. This is the reason why it is suggested to transport smooth

pseudoconcentration functions in order to avoid numerical oscillations.^{4,17} We believe that it is possible to transport a discontinuous pseudoconcentration provided that the discontinuous Galerkin method is used to solve (12).^{7,18,19} As discussed in Reference 18, the discontinuous Galerkin method is among the best in that case. Very sharp discontinuous solutions can be computed at the price of very-small-amplitude wiggles in the vicinity of the discontinuities. These wiggles do not prevent accurate prediction of interfaces and do not generate numerical instabilities.

One of the main features of this method is that it allows the solution of (12) on an element-by-element basis. Indeed, since S is discontinuous, it seems natural to use discontinuous approximations and to define

$$V_h = \{w | w|_K \in P_k(K), \forall K \in \mathcal{T}_n\}, \quad (27)$$

where K is an element of the triangulation and $P_k(K)$ is the set of polynomials of degree k on element K . It is important to remark that no continuity is required at element interfaces. This choice is partly motivated by the fact that the solution S is inevitably discontinuous and has the form

$$S = \begin{cases} 1 & \text{if } \tilde{x} \in \Omega_1, \\ 0 & \text{if } \tilde{x} \in \Omega_2. \end{cases} \quad (28)$$

The discontinuous Galerkin method¹⁸ takes the following form. On each element K solve

$$\int_K \tilde{u} \cdot \vec{\nabla} S \omega \, d\Omega - \int_{\partial K^-} S(\tilde{u} \cdot \tilde{n}) \omega \, dS = - \int_{\partial K^-} S^-(\tilde{u} \cdot \tilde{n}) \omega \, dS \quad \forall \omega \in P_k(K). \quad (29)$$

Referring to Figure 4, since the approximation is discontinuous at element interfaces, S^- is the value of S in the element adjacent to K on the inflow part ∂K^- of the boundary of element K . More precisely, let us define

$$\partial K^- = \{\tilde{x} \in \partial K | \tilde{u}(\tilde{x}) \cdot \tilde{n}(\tilde{x}) < 0\}, \quad (30)$$

$$S = \lim_{\varepsilon \rightarrow 0} S(\tilde{x} + \varepsilon \tilde{u}) \quad (\tilde{x} \in \partial K^-), \quad (31)$$

$$S^- = \lim_{\varepsilon \rightarrow 0} S(\tilde{x} - \varepsilon \tilde{u}) \quad (\tilde{x} \in K^-). \quad (32)$$

An important feature of the discontinuous Galerkin method is that equation (29) results in a small linear system on each element. It can be easily solved on element K , but only if S^- has

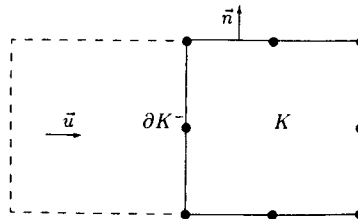
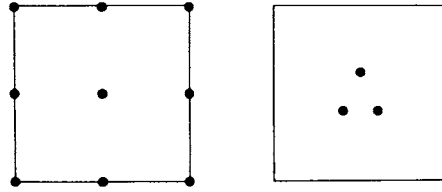


Figure 4. Two adjacent elements

Figure 5. $Q_2^0 - P_1$ element

already been computed. This implies that the elements must be solved in a proper order. Such an order usually exists¹⁹ when there is no recirculation zone. The idea is to start with elements adjacent to $\partial\Omega^-$ and follow the flow field \tilde{u} . A good numbering of the elements (in accordance with the flow) accelerates the convergence but is not essential for convergence. If the numbering is not optimal or if there exists a recirculation zone in the flow field, the elements can be swept many times until convergence. The discontinuous Galerkin method is then a block Gauss–Seidel method.

4. ALGORITHMS

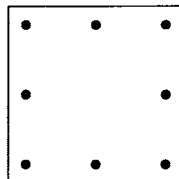
In this case the Picard algorithm becomes as follows.

1. For a given value of S the rheological constants in the Carreau model can be deduced at each Gauss point and the Stokes problem (5), (6) is solved with the algorithm (25).
2. For a given value of \tilde{u} the transport equation (12) is solved using the algorithm (29) to get a new value of S denoted S^{new} .
3. If $\|S - S^{\text{new}}\| < \epsilon$, stop; else $S = S^{\text{new}}$ and go to step 1.

4.1. Discretization

The three variables to discretize are the velocity \tilde{u} , the pressure p and the pseudoconcentration S . For the velocity and pressure the $Q_2^0 - P_1$ quadratic element was used. Figure 5 illustrates this element. This element satisfies the Ladyzenskaya–Babuška–Brezzi (LBB) condition^{20,21} and is one of the best two-dimensional elements.

For the pseudoconcentration function S the Q_2^8 element depicted in Figure 6 was chosen. A Q_1 approximation can also be used, but the quadratic element provided the best results. This choice was motivated by our experience with viscoelastic fluid flow problems where a transport equation has to be solved for the stresses. An LBB condition also exists in that case which is satisfied by the above discretizations.²²

Figure 6. The Q_2^8 element

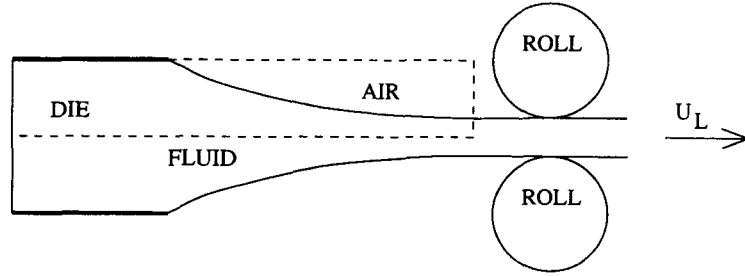


Figure 7. Schematic view of film casting

5. THE FILM-CASTING PROBLEM

In this section we briefly indicate how the developed methodology can be modified for the simulation of the film-casting process. Figure 7 gives a schematic view of the problem. We define the draw ratio

$$Dr = U_L / \bar{U}, \quad (33)$$

with U_L the draw velocity and \bar{U} the average velocity of the flow at the die exit. As we will see, the stability of the interface (between fluid and air) depends on this draw ratio. The dashed line of Figure 7 corresponds to the domain illustrated in Figure 8.

As can be easily seen, the problem is similar to coextrusion with air playing the role of the second polymer. Following Reference 17, air is considered as an incompressible fluid of very low viscosity. The imposed boundary conditions are

$$\begin{aligned} \vec{u} &= Q(u_0(y), 0), \quad \vec{x} \in \Gamma_e, \\ \vec{u} &= 0, \quad \vec{x} \in \Gamma_0, \\ \sigma_2 \cdot \vec{n} &= 0, \quad \vec{x} \in \Gamma_h, \\ u_2 &= 0 \quad \text{and} \quad (\sigma_1 \cdot \vec{n})_x = 0, \quad \vec{x} \in \Gamma_b, \\ \vec{u} &= (U_L, 0), \quad \vec{x} \in \Gamma_s. \end{aligned} \quad (34)$$

At the die entry Γ_e , a half-parabola with flow rate Q is imposed. A no-slip condition is imposed on Γ_0 , while the flow (and thus the interface) is supposed fully developed with $\vec{u} = (U_L, 0)$ (the draw velocity) on Γ_s . Γ_b is a symmetry axis.

As in the coextrusion problem, a value of the pseudoconcentration is imposed at the entrance of the domain Γ_e . Its value will be transported in all the domain by the velocity field. We choose

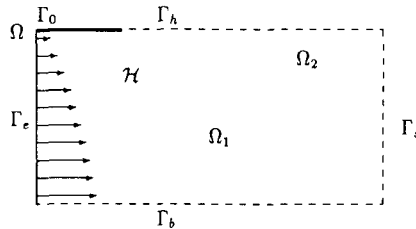


Figure 8. Boundary conditions for film casting

the following function:

$$S = 1 \quad \text{if } \tilde{x} \in \Gamma_e. \quad (35)$$

Moreover, a velocity profile will be computed in the air (in Ω_2). Consequently, it is possible that $\tilde{u} \cdot \tilde{n} < 0$ on Γ_h and thus a boundary condition for S must be provided there when necessary. When this is the case, S is fixed to zero on Γ_h .

Here again the jump in the function will give the position of the interface between fluid and air.

5.1. The free surface condition

The free surface condition

$$\sigma_1 \cdot \tilde{n} = 0, \quad \tilde{x} \in \mathcal{H}, \quad (36)$$

is treated as a particular case of (17). Indeed, if we consider $\sigma_2 \cdot \tilde{n}$ in the air,

$$\sigma_2 \cdot \tilde{n} = p_2 \tilde{n} + \tau_2 \cdot \tilde{n}. \quad (37)$$

However, since the viscosity of air is supposed very small with respect to that of the polymer, $\tau_2 \cdot \tilde{n} \simeq 0$. Moreover, equation (1) gives

$$\nabla p_2 = 0, \quad (38)$$

which implies that $p_2 = \text{constant}$ in Ω_2 . From the condition $\sigma_2 \cdot \tilde{n} = 0$ on Γ_h we conclude that $p_2 = 0$ and thus $\sigma_1 \cdot \tilde{n} \simeq 0$

5.2. Solution algorithm

Both stationary and time-dependent solutions can be computed for this problem. For stationary solutions the same algorithm (see Section 4) as for the coextrusion problem is used.

For time-dependent solutions the transport equation is given by (11) where the time derivative is discretized by the fully implicit Gear scheme (13). The Picard iterative scheme of Section 4 then has to be used at each time step.

6. NUMERICAL RESULTS

The results for the coextrusion and film-casting problems are now presented. In both cases the computations are started on a uniform mesh. When necessary, the mesh can be concentrated in some regions of the domain in a very simple manner. For example, in the coextrusion problem a solution is computed on a uniform mesh, and if one of the fluid layers is very small, the mesh is concentrated in the vicinity of that layer and a new computation is performed on the new mesh. This can be seen as a very primitive adaptive method. It is, however, easy to conceive a more sophisticated adaptive strategy where one has to locate the discontinuity of the function S to decide where to refine the mesh. This strategy was not implemented in this work.

For the coextrusion problem, simulations with up to five different fluids are presented. For the film-casting problem the main difficulty is to catch the movement of the interface in time. As we shall see, a Hopf bifurcation depending on the draw ratio and on the power index of the Carreau model occurs.

Table I. Rheological parameters and flow rates (220 °C)

Model	Polymer	η_0 (Pa s)	λ (s)	n	c	Flow rate
Carreau	ABS (lower)	8597	0.096	0.290	1	130
	Adheflon (middle)	7381	0.101	0.338	1	3.5
	PVDF (upper)	5224	0.093	0.443	1	10
Power law	ABS (lower)	45425	1	0.290	0	130
	Adheflon (middle)	33896	1	0.338	0	3.5
	PVDF (upper)	19601	1	0.443	0	10
Newton	ABS (lower)	8597	1	1	0	130
	Adheflon (middle)	7381	1	1	0	3.5
	PVDF (upper)	5224	1	1	0	10

6.1. Coextrusion

The first example is the coextrusion of three polymers. This is a typical example where two polymers are coextruded and joined together by an adhesive. The adhesive is also a polymer but its width is very small compared with the two polymers. The rheological parameters for the different models are given in Table I. They correspond to a realistic coextrusion problem.²¹

The starting mesh is illustrated in Figure 9, consisting of 30 elements in the y -direction and 40 elements in the x -direction. The dimension of the domain is 1×1.6667 .

Starting with this uniform mesh, the interfaces were computed quite accurately, but owing to the coarse mesh, the adhesive layer fell within one element width. To improve the accuracy, the mesh was concentrated in the vicinity of the adhesive layer, resulting in the mesh of Figure 10.

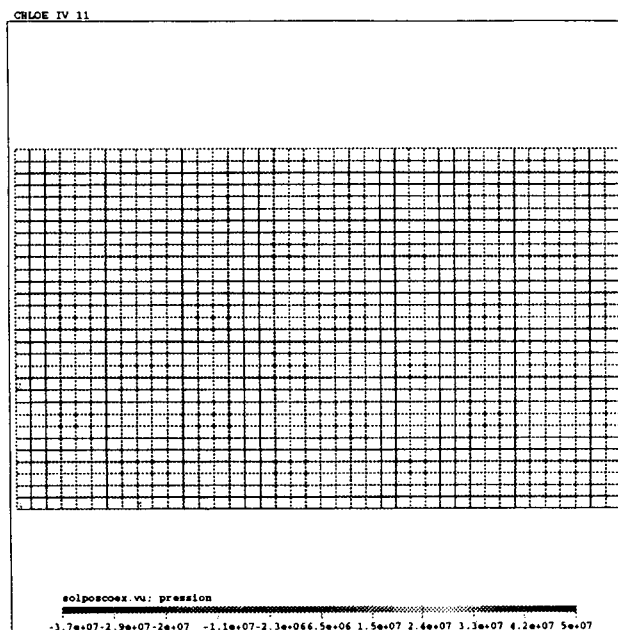


Figure 9. Uniform mesh for coextrusion

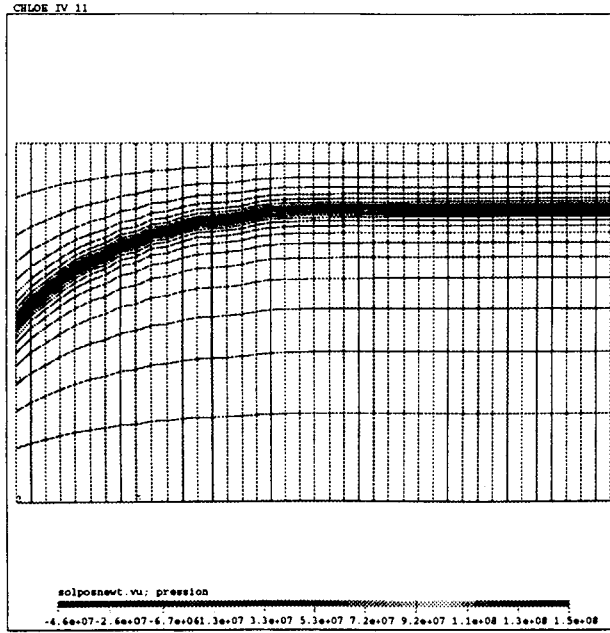


Figure 10. Adapted mesh for coextrusion

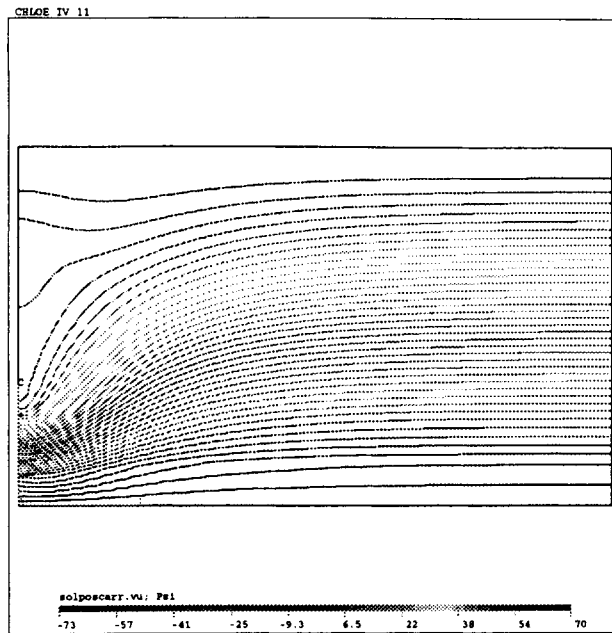


Figure 11. Streamlines for Carreau fluids (three polymers)

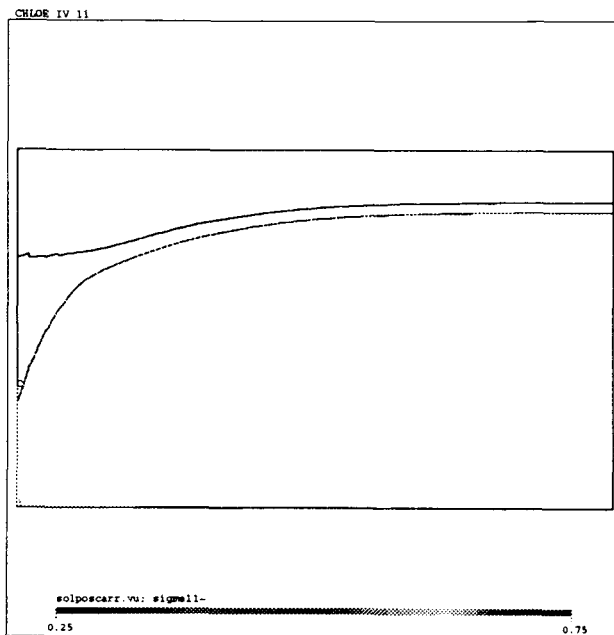


Figure 12. Interface position for Carreau fluids (three polymers)

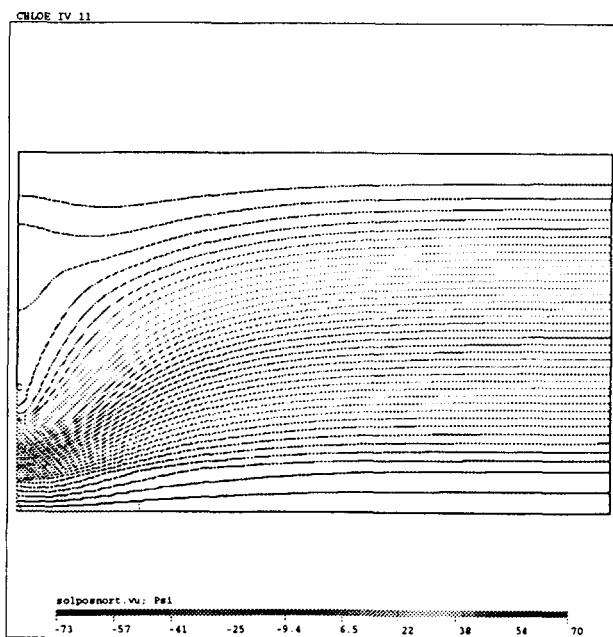


Figure 13. Streamlines for power law fluids (three polymers)

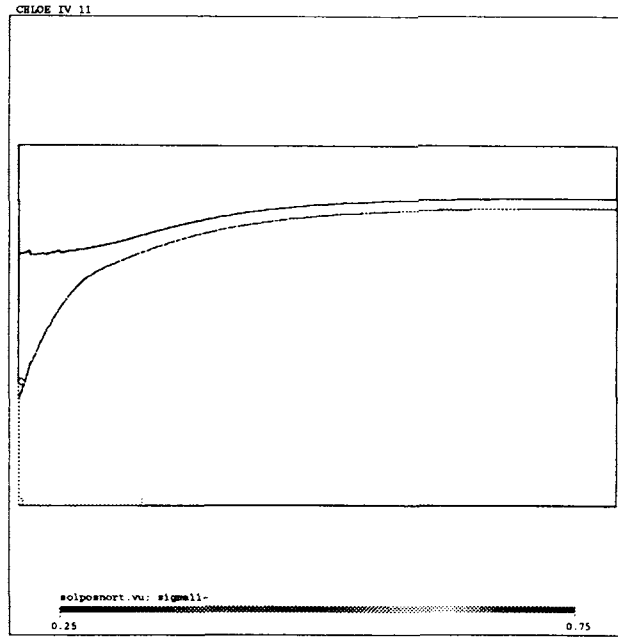


Figure 14. Interface position for power law fluids (three polymers)

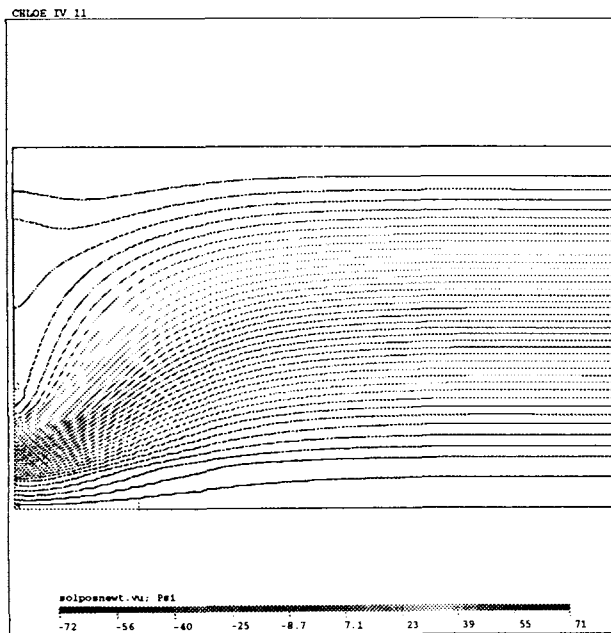


Figure 15. Streamlines for Newtonian fluids (three polymers)

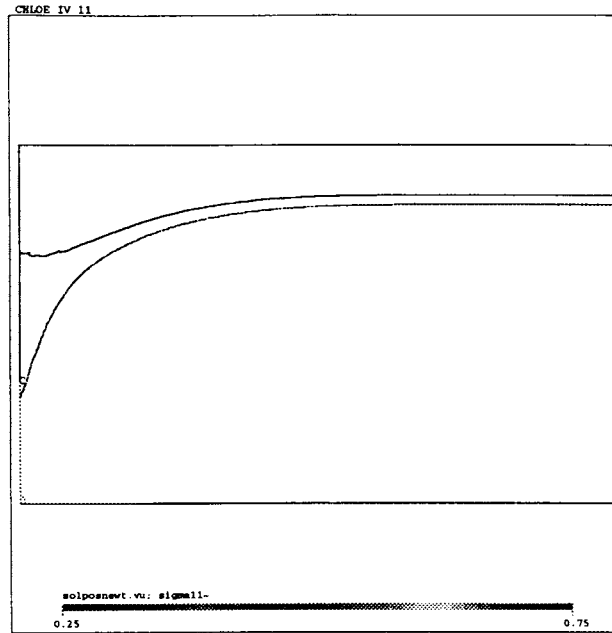


Figure 16. Interface position for Newtonian fluids (three polymers)

Figures 11–16 show the solutions obtained with the three models: Carreau, power law and Newtonian. Streamlines and interfaces positions are presented, showing no fundamental difference between the three models.

A cross-section of the pseudoconcentration S at $x = 1.667$ (Figure 17) allows us to compare the interface positions for the three models. The three plateaus give the positions of the different fluids. Only slight differences can be seen. Small oscillations are present but do not prevent an

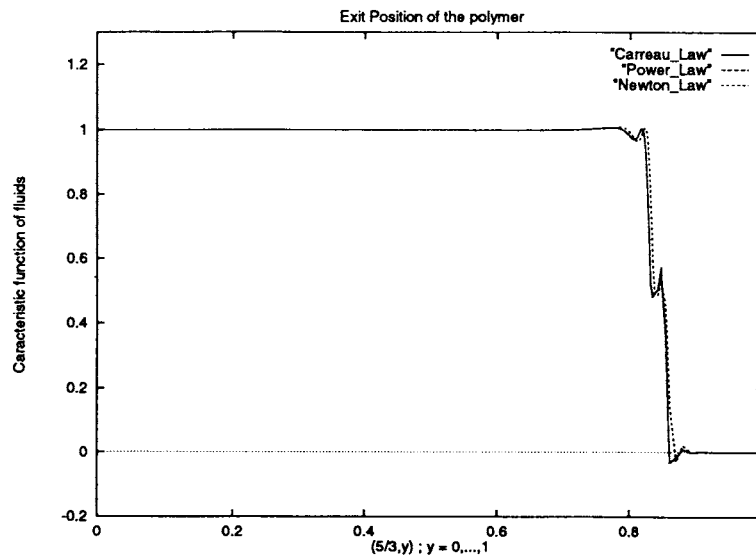


Figure 17. Exit section of pseudoconcentration

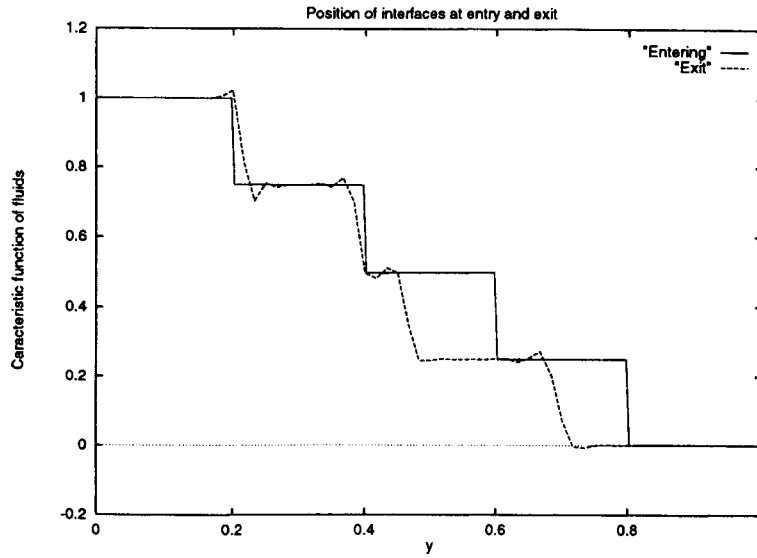


Figure 18. Entry and exit sections of pseudoconcentration

accurate estimation of the interface positions. As explained in Reference 18, other methods would add numerical diffusion and the plateau corresponding to the adhesive would be lost.

Finally, a simulation with five polymers has been conducted. The uniform grid of Figure 9 and the Newtonian model were used. The constant viscosities are those given in Table I. The polymers ABS, Adheflon, PVDF, Adheflon and ABS are ordered from bottom to top of the domain with respective flow rates of 10, 20, 10, 30 and 20 (adimensional units).

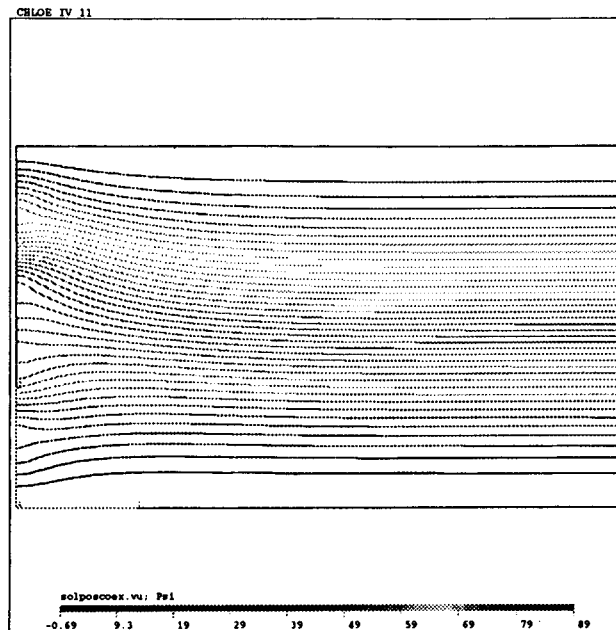


Figure 19. Streamlines for Newtonian fluids (five polymers)

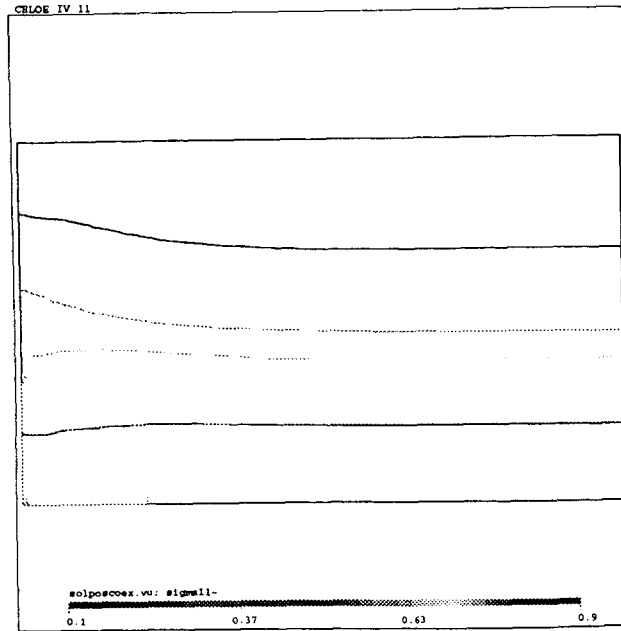


Figure 20. Interface position for Newtonian fluids (five polymers)

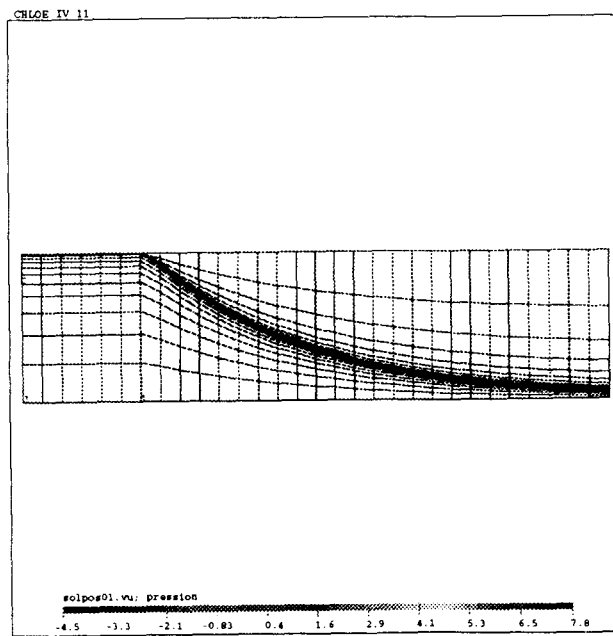


Figure 21. Mesh for film casting

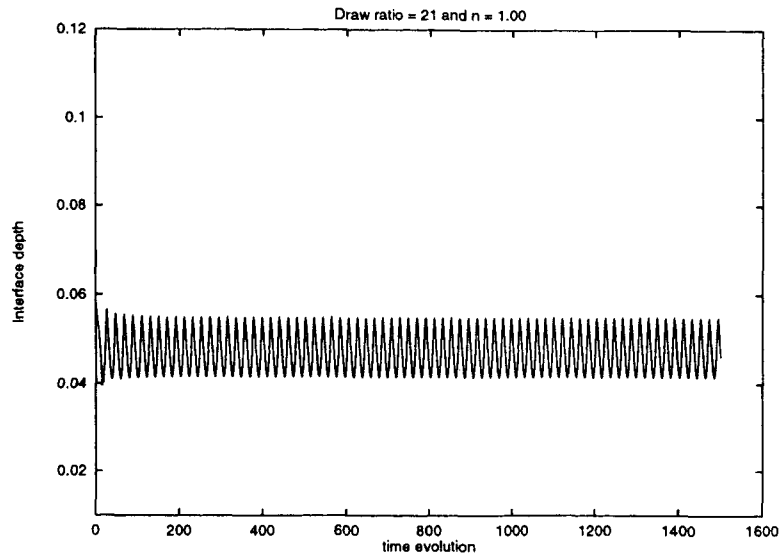


Figure 22. Time-dependent film width; $Dr = 21$, $n = 1.00$

Figure 18 shows the pseudoconcentration at the entry ($x = 0$) and exit ($x = 1.667$) sections of the domain. This figure allows us to compare the initial and final positions of the different fluids. Streamlines and interface positions are presented in Figures 19 and 20.

6.2. Film casting

The solution strategy for the film-casting problem is similar to the one used in the coextrusion problem. The dimension of the computational domain is 1×24 adimensional units (the die is 4 units long). In the following the figures have been contracted by a factor of six in the x -direction,

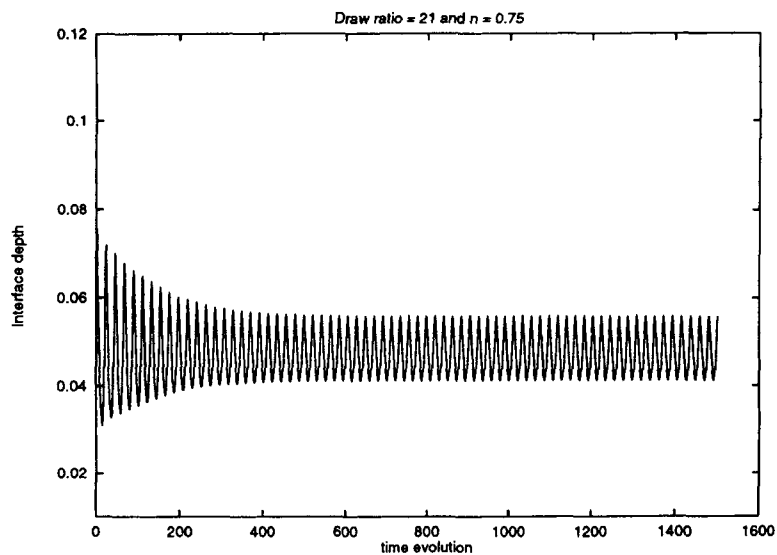
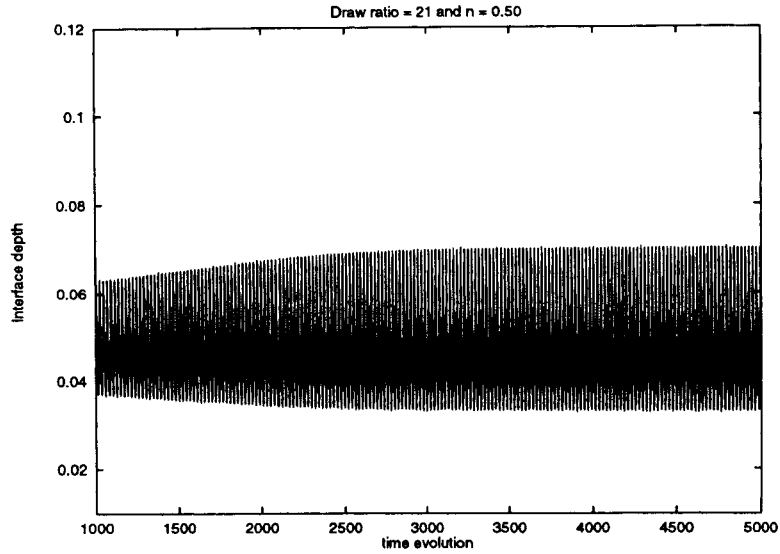
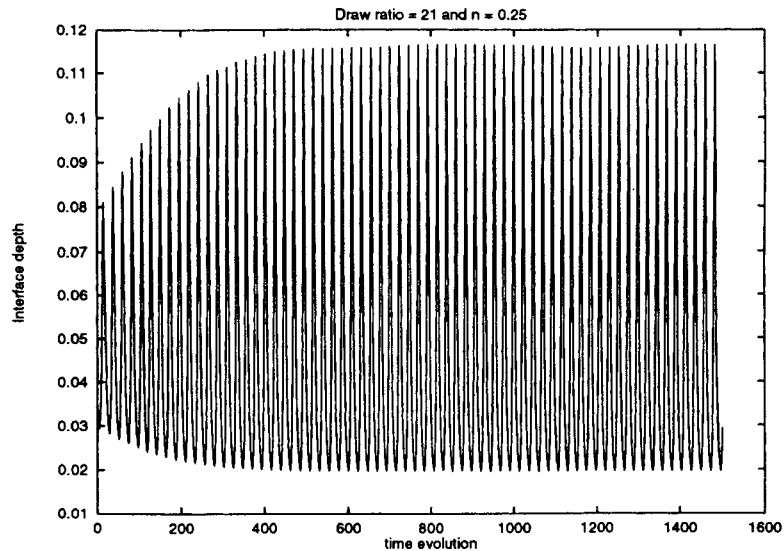


Figure 23. Time-dependent film width; $Dr = 21$, $n = 0.75$

Figure 24. Time-dependent film width; $Dr = 21$, $n = 0.50$

because it is barely possible to see anything when using the original dimension. Starting with a uniform mesh of 20 elements in the y -direction and 30 elements in the x -direction, a solution is computed for a Newtonian fluid and the mesh is concentrated in the vicinity of the free surface (Figure 21). A new computation is then performed. It is worth noticing that the solution on the uniform mesh is already acceptable, but since our concern is the time-dependent case which results in small-amplitude oscillations, we felt it necessary to concentrate the mesh. This mesh is not very elegant, but it concentrates the mesh in the critical region.

Figure 25. Time-dependent film width; $Dr = 21$, $n = 0.25$

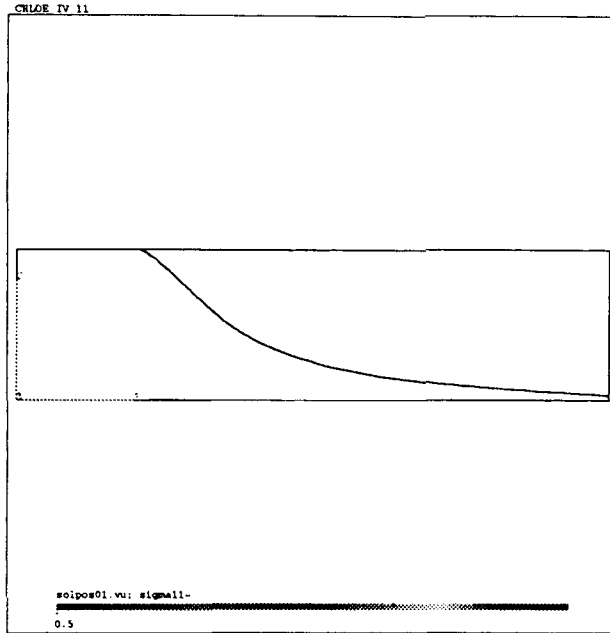


Figure 26. Interface position at time T_0

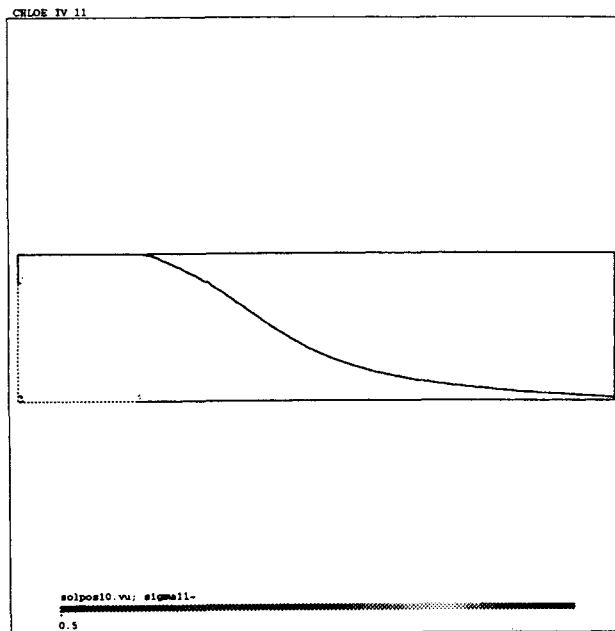
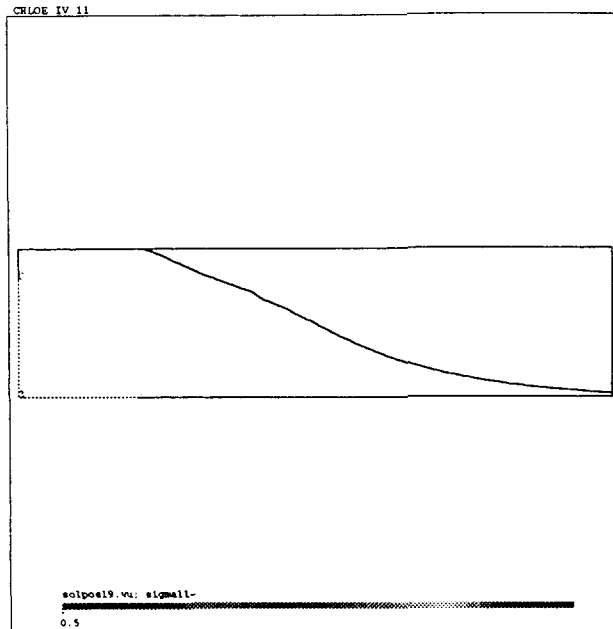
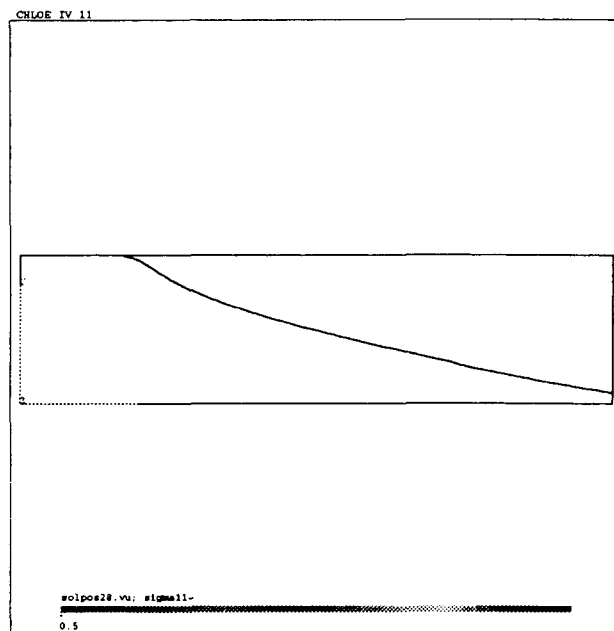


Figure 27. Interface position at time $T_0 + 4.5$

Figure 28. Interface position at time $T_0 + 90$ Figure 29. Interface position at time $T_0 + 13.5$

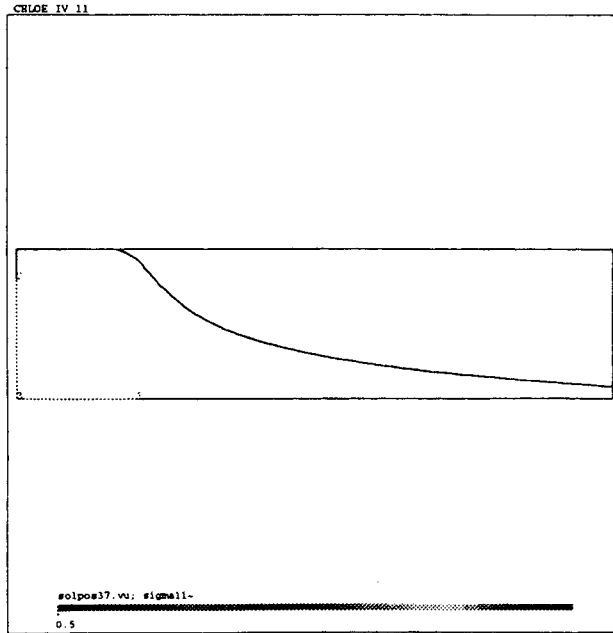


Figure 30. Interface position at time $T_0 + 18$

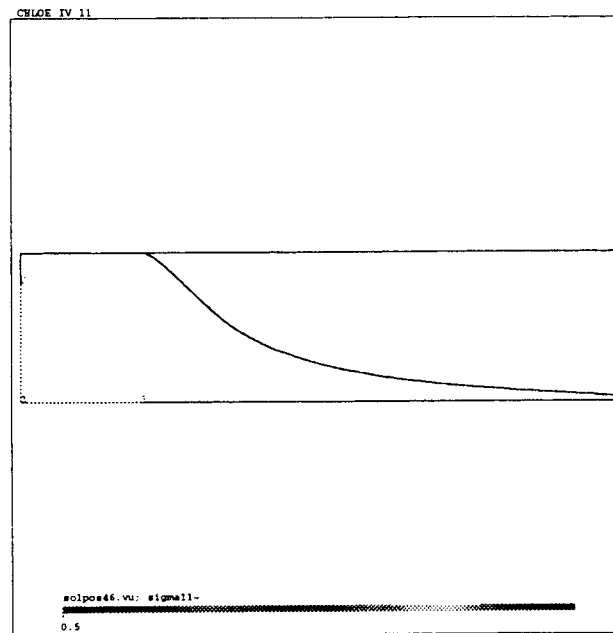
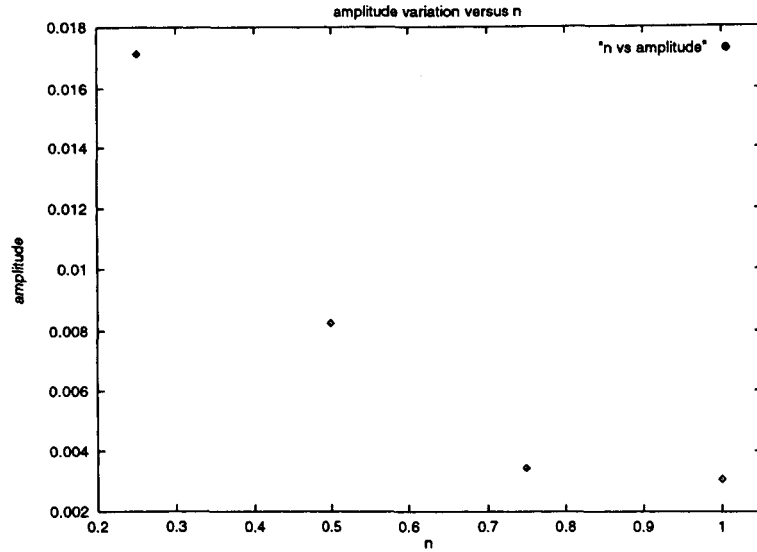
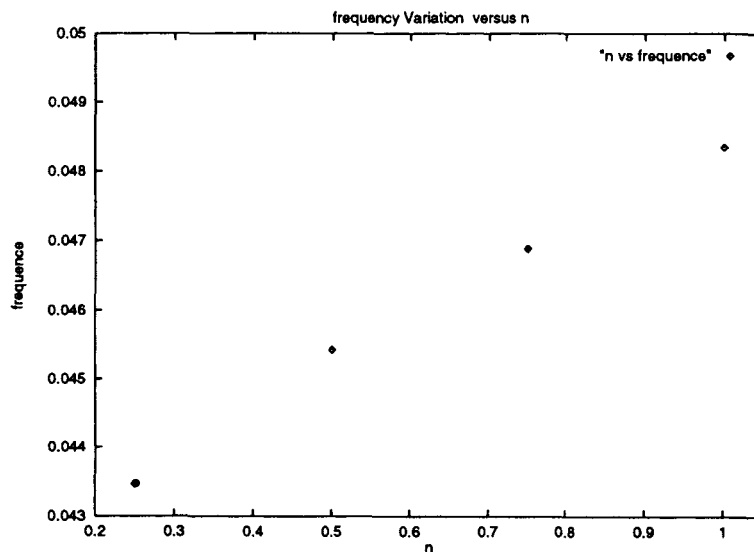


Figure 31. Interface position at time $T_0 + 22.5$

Figure 32. Variation in amplitude with n

The draw ratio is then slowly increased and stationary solutions are obtained up to $Dr = 20$. From now on the mesh will be kept fixed. It is well known¹³ that this problem becomes time-dependent at a draw ratio around 21 in the Newtonian case ($n = 1$). Indeed, a Hopf bifurcation occurs and the free surface starts oscillating. The width of the film at the exit section varies with time as shown in Figure 22. The next figures show the influence of the Carreau parameter n on the amplitude of the oscillations. Results are presented for $n = 0.75, 0.5$ and 0.25 (Figures 23–25 respectively). A typical time-dependent free surface is illustrated in Figures 26–31.

Figure 33. Variation in frequency with n

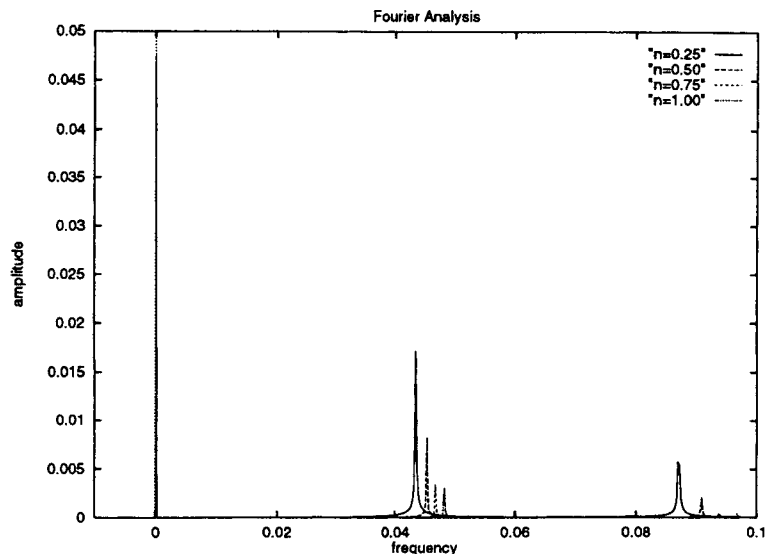
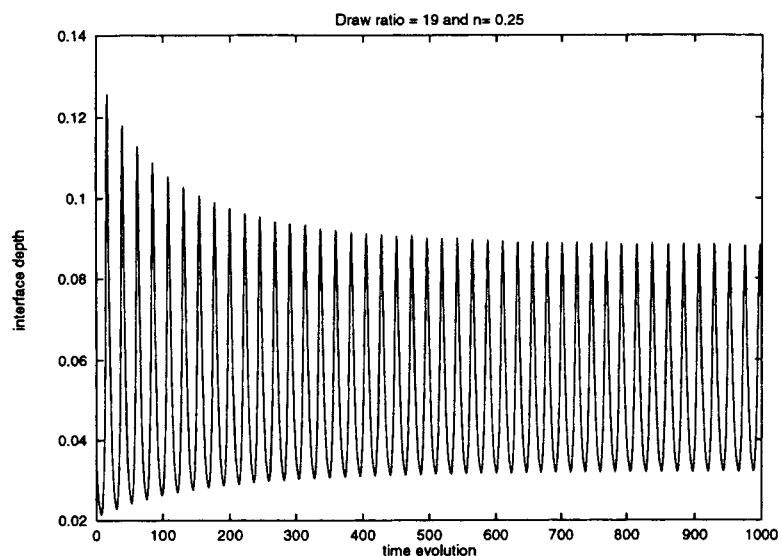


Figure 34. Fourier analysis

The pulsating nature of the flow is easily seen by looking at the swelling of the free surface and the variation in the film width at the exit section.

It is clear that shear thinning has a strong influence on the amplitude and a moderate one on the frequency, as can be seen in Figures 32 and 33 respectively. This is confirmed by the Fourier analysis of Figure 34. As n decreases, the amplitude of the oscillations increases while the frequency decreases.

Finally, we have investigated the influence of shear thinning on the critical draw ratio where the Hopf bifurcation occurs. For $n = 0.25$, starting from the solution at $Dr = 21$, the draw ratio

Figure 35. Evolution to a time-dependent solution; $Dr = 19$

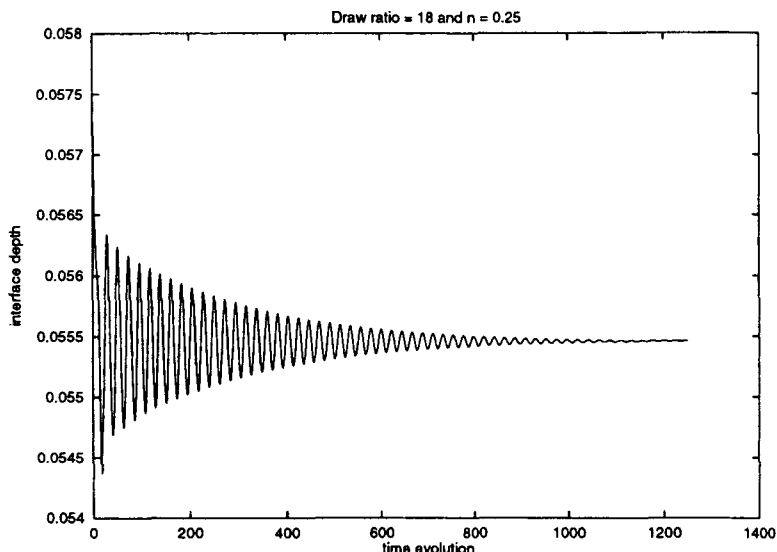


Figure 36. Evolution to a stationary solution; $Dr = 18$

was slowly decreased until the solution became stationary. At $Dr = 19$ the solution is still time-dependent, as can be seen in Figure 35. The solution is, however, stationary at $Dr = 18$ (Figure 36) and the critical draw ratio is thus somewhere around $Dr = 18.5$. It is therefore concluded that film casting of shear-thinning fluids will become unstable at a lower draw ratio.

7. CONCLUSIONS

This paper presents a numerical simulation of the coextrusion and film-casting processes. The developed numerical method allows the computation of both stationary and time-dependent free surfaces in an efficient manner.

The results for film casting and coextrusion with up to five polymers show the flexibility of the algorithm. This opens the door to the investigation of the influence of the models and rheological parameters on different polymer processes where free surfaces frequently occur.

A three-dimensional version of the present method is currently under development.²⁴ Our goal is to study encapsulation, which is a purely three-dimensional phenomenon where the less viscous fluid tends to encapsulate (lubricate) the more viscous one. Linear stability for this problem has been studied in Reference 25. Preliminary results show that encapsulation can be captured by our method.

ACKNOWLEDGEMENTS

This work was partly supported by NSERC (Canada) and by FCAR (Québec).

REFERENCES

1. J. F. Agassant, A. Fortin, Y. Demay, 'Prediction of stationary interfaces in coextrusion flows', *Polym. Eng. Sci.*, **34**, 1101–1108 (1994).
2. M. J. Crochet, V. Delvaux and J. M. Marchal, 'Numerical prediction of viscoelastic extrudate swell', *NUMIFORM 89*, Balkema, Rotterdam, 1989, pp. 17–22.
3. C. W. Hirt and B. D. Nichols, 'Volume of fluid (VOF) method for the dynamics of free boundaries', *J. Comput. Phys.*, **39**, 201–225 (1981).

4. E. Thompson, 'Use of pseudo-concentrations to follow creeping viscous flows during transient analysis', *Int. j. numer. methods fluids*, **6**, 749–761 (1986).
5. S. F. Shen, 'Grapplings with the simulation of non-Newtonian flows in polymer processing', *Int. j. numer. methods eng.*, **34**, 701–723 (1992).
6. P. Carrier, 'Calcul des surfaces libres de procédés de mise en forme des polymères', *Mémoire*, École Polytechnique de Montréal, 1993.
7. A. Fortin, Y. Demay and J. F. Agassant, 'Computation of stationary interface between generalized Newtonian fluids', *Rev. Eur. Éléments Finis*, **1**, 181–196 (1992).
8. J. F. Agassant, P. Avenas, J. P. Sergent and P. Carreau, *Polymer Processing, Principles and Modeling*, Carl Hanser, pp. 1–40.
9. R. B. Bird, R. C. Armstrong and O. Hassager, *Dynamics of Polymer Liquids*, Wiley, New York, 1977.
10. E. Thompson and R. E. Smelser, 'Transient analysis of forging operations by the pseudo-concentration method', *Int. j. numer. methods engng*, **25**, 177–189 (1988).
11. J. M. Ottino, *Cambridge Texts in Applied Mathematics*, Cambridge University Press, Cambridge, 1989.
12. P. Barq, J. M. Haudin, J. F. Agassant, H. Roth and P. Bourgin, 'Instability phenomena in film casting process', *Int. Polym. Process.*, **V**, 264–271 (1990).
13. Y. Demay and J. F. Agassant, 'Experimental study of the draw resonance in fiber spinning', *J. Non-Newtonian Fluid Mech.*, **18**, 187–198 (1985).
14. A. Fortin, M. Fortin and J. J. Gervais, 'A numerical simulation of the transition to turbulence in a two-dimensional flow', *J. Comput. Phys.*, **70**, 295–310 (1987).
15. M. Fortin and A. Fortin, 'A generalization of Uzawa's algorithm for the solution of the Navier–Stokes equations', *Commun. Appl. Numer. Methods*, **1**, 205–208 (1985).
16. M. Fortin and R. Glowinski, 'Résolution numérique de problèmes aux limites par des méthodes de lagrangien augmenté', *Colloq. Math., Sér. Math. Pures Appl.*, Département de Mathématiques, Université Laval, 19XX.
17. G. Dhatt, D. M. Gao and A. Ben Cheikh, 'A finite element simulation of metal flow in moulds', *Int. j. numer. methods eng.*, **30**, 821–831 (1990).
18. C. Johnson, *Numerical Solution of Partial Differential Equations by the Finite Element Method*, Cambridge University Press, Cambridge, 1990.
19. D. Pelletier, A. Zaki and A. Fortin, 'Adaptive remeshing for hyperbolic transport problems', *J. Fluid Dyn.*, submitted.
20. Brezzi and M. Fortin, *Mixed and Hybrid Finite Element Methods*, Springer, New York, 1990.
21. M. Fortin and A. Fortin, 'Experiments with several elements for viscous incompressible flows', *Int. j. numer. methods fluids*, **5**, 911–928 (1985).
22. A. Fortin, A. Zine and J. F. Agassant, 'Computing viscoelastic fluid flow problems at low cost', *J. Non-Newtonian Fluid Mech.*, **45**, 209–229 (1992).
23. S. Puissant, 'Etude numérique et expérimentale de la coextrusion des polymères dans une filière plate', *Thèse*, Ecole Nationale Supérieure des Mines de Paris, 1992.
24. A. Fortin, J. Teixeira, Y. Demay and J. F. Agassant, in preparation.
25. D. D. Joseph, M. Renardy and Y. Renardy, 'Instability of the flow of two immiscible liquids with different viscosities in a pipe', *J. Fluid Mech.*, **141**, 309–317 (1984).
26. A. Zaki, 'Simulation numérique de problèmes de convection sur des maillages adaptatifs non-structurés du type h-p', *Thèse*, Ecole Polytechnique de Montréal, 1993.